Molecular Basis for the Origin of Differential Spectral and Binding Profiles of Dansylamide with Human Carbonic Anhydrase I and II†

Abir L. Banerjee, Shakila Tobwala, Bratati Ganguly, Sanku Mallik, and D. K. Srivastava*

Department of Chemistry and Molecular Biology, North Dakota State University, Fargo, North Dakota 58105

Received November 28, 2004; Revised Manuscript Received January 7, 2005

ABSTRACT: Sulfonamide derivatives serve as potent inhibitors of carbonic anhydrases (CAs), and a few such inhibitors have been currently used as drugs for the treatment of different pathogenic conditions in humans. In pursuit of designing the isozyme-specific inhibitors of human CAs, we observed that the fluorescence spectral properties and binding profiles of a fluorogenic sulfonamide derivative, 5-(dimethylamino)-1-naphthalenesulfonamide (dansylamide, DNSA), were markedly different between the recombinant forms of human carbonic anhydrase I (hCA I) and II (hCA II). The kinetic evaluation of the overall microscopic pathways for the binding of DNSA to hCA I versus hCA II revealed that the protein isomerization step served as a major determinant of the above discrepancy. Arguments are presented that the detailed structural−functional investigations of enzyme−ligand interactions may provide insights into designing the isozyme-specific inhibitors of CAs.

In the present proteomics era, there has been major thrust in determining the structures of proteins and their complexes with small molecular weight ligands via X-ray crystallography and NMR methods (*1*−*3*). Such structural details are conceived to facilitate the ultimate goal of designing drugs for the treatments of diverse pathological conditions in humans (*4*). Implicit in the advancement of structural-biology-related research is the hope of rationally designed small molecular weight ligands with predetermined affinities for macromolecules (*5*−*6*). Currently, there are about 28 000 structures of biological macromolecules available in the Protein Data Bank, and this list is growing by about 4500 new structures per year. Despite the availability of high-resolution structures of enzymes, the ability to design complementary ligands, which could perfectly fit to the active-site pockets and serve as potent inhibitors, are highly limited. This limitation is intrinsic to the complex structural−functional relationships of enzyme−ligand interactions and catalysis (*4*−*5*).

Because of enforcement of their three-dimensional structures by noncovalent interactions, the enzyme structures are highly flexible. Such flexibility is important for maximizing the interactions of enzymes with their cognate substrates in the ground states, eliciting enzyme−substrate specificity, optimizing the flanking transition-state structures, and helping to release the products via an increase in the motion of the intervening flap/domain structures (*7*−*8*). These features remain obscured on examination of the static X-ray crystallographic structures of enzymes in the absence and presence of their cognate ligands (*5*). The coupling between protein conformational changes and enzyme catalysis is poorly understood, and this feature becomes further complicated if the enzyme catalysis proceeds via multiple steps (*9*).

In pursuit of designing the enzyme inhibitors against pathogenic enzymes, we became interested in the molecular basis of isozyme selectivity in carbonic anhydrases (CAs)[1] (*10*−*12*). In animal kingdom, there are 15 isozymes of CAs, of which five isozymes (CA I, CA II, CA III, CA VII, and CA XIII) are cytoplasmic, two (CA VA and CA VB) are mitochondrial, one (CA VI) is secreted, four (CA IV, CA IX, CA XII, and CA XIV) are membrane-associated, and the remaining three (CA VIII, CA X, and CA XI) are "noncatalytic" in nature (*13*−*14*). Of these, CA VIII, CA IX, and CA XII have been recognized to be involved in tumorigenesis (*15*). Except for "noncatalytic" CAs, all of the above isozymes are involved in reversible hydration of CO_2 to form HCO_3^-, which is involved in a variety of biosynthetic reactions (*16*), such as gluconeogenesis, synthesis of certain amino acids (via pyruvate carboxylase), lipogenesis (via acetyl-CoA carboxylase), ureagenesis (via carbamoyl phosphate synthetase I), and pyrimidine nucleotide biosynthesis (via carbamoyl phosphate synthetase II). Besides, these enzymes are involved in the pH homeostasis, ion transport, water and electrolyte balance, bone resorption, calcification, and tumorigenesis (*17*).

Because of their involvement in different physiological processes, CAs have been the target of drug design for last 50 years, and a variety of highly potent inhibitors initially emerged as drugs for the treatment of different pathological conditions, such as glaucoma, hypertension, convulsion and epilepsy, altitude sickness, obesity, diabetes, etc. (*18*−*23*). However, because of serious side effects, several highly potent CA inhibitors could not pass scrutiny at different stages of clinical trials, and several approved drugs were subsequently withdrawn from the market (*13*, *24*). Currently,

† This research was supported by the National Institutes of Health Grants 1R15 HL077201-01 to D.K.S. and 1R01 GM 63404-01A1 to S.M.

* To whom correspondence should be addressed. Telephone: 701-231-7831. Fax: 701-231-7884. E-mail: dk.srivastava@ndsu.nodak.edu.

[1] Abbreviations: CA, carbonic anhydrase; hCA I, human carbonic anhydrase I; hCA II, human carbonic anhydrase II; DNSA, dansylamide.

10.1021/bi0475018 CCC: $30.25
Published on Web 02/11/2005

dorzolamide and brinzolamide are only two CA inhibitors that have been approved for topical applications for the treatment of chronic glaucoma (*14*).

We recently devised a two-prong methodology for designing highly potent and isozyme-specific inhibitors of CAs (refs *10*−*12* and patent pending). Our methodology relies on enhancing the binding affinity of an active-site-directed ligand (e.g., benzenesulfonamide) by attaching an iminodiacetate (IDA)-Cu^{2+} as a tether residue, which loops around and interacts at the surface-exposed histidine residue of the enzyme (*10*−*12*). Because the surface-exposed histidine residues differ from one isozyme to the other, our approach has potential of designing the isozyme-specific inhibitors of CAs, and possibly of other pathogenic enzymes.

A casual perusal of literature data on CA inhibitors reveal that a majority of sulfonamide derivatives serve as more potent inhibitor to CA II than to CA I (*26*−*27*). This is in marked contrast to our preliminary data that indicate that 5-(dimethylamino)-1-naphthalenesulfonamide (dansylamide) binds more tightly to hCA I than to hCA II. It has been reported that the fluorescence emission maximum of free dansylamide (in water) is blue-shifted from 580 to 468 nm upon binding with bovine CA with a concomitant increase in the quantum yield from 0.055 to 0.84 (*34*). The quantum yield of dansylamide is about 4-fold higher when bound to hCA I than to hCA II. The question arose whether the above physical differences were encoded by some common molecular mechanism. If so, can such molecular mechanism be utilized to rationally design the isozyme-specific inhibitors of the enzyme? The anomalous binding affinity of dansylamide for hCA I versus hCA II (see above) appeared to be corroborated by the fact that the above ligand binds at the bovine CA II site in an unusual mode, which is different from any other enzyme-bound sulfonamide derivative, characterized by the X-ray crystallographic studies (*28*). To ascertain the structural−functional aspects of the difference in the spectral and binding profiles of dansylamide to hCA I versus hCA II, we performed detailed ligand binding and transient kinetic experiments. The experimental data reveal that the origin of the above differences lies in the difference in the sequence of steps (referred to as the microscopic pathways) of the enzyme−ligand interactions.

EXPERIMENTAL PROCEDURES

Materials. Zinc sulfate, ampicillin, chloramphenicol, Tris, and IPTG were purchased from Life Science Resources, Milwaukee, WI; yeast extracts and tryptone were purchased from Becton Dickinson, Sparks, MD; acetonitrile was from Aldrich Chemicals, Milwaukee, WI; HEPES, *p*-aminomethylbenzenesulfonamide-agarose, *p*-nitrophenyl acetate, HEPES, MES, and PMSF were obtained from Sigma; and dansylamide was purchased from Avocado Research Chemicals, Heysham, Lancashier, U.K. The plasmid containing the coding sequence of hCA I (pCMV-SPORT6) was obtained from Open Biosystems, Huntsville, AL. The expression cells BL21 codon plus DE3(RIL) was from Stratagene, La Jolla, CA. All other chemicals were of reagent grade and were used without further purification.

General Methods: Cloning Expression and Purification of the Recombinant Human Carbonic Anhydrase I (hCA I). The coding sequence of hCA I (plasmid, pCMV-SPORT6) was amplified by the hot-start PCR method (*29*) using the sense and anti-sense primers, 5′-GGAATTCCATATG-GCAAGTCCAGACTGGG-3′and 5′-CCGCTCGAGTTAA-AATGAAGCTCTCACTGTTC-3′, respectively. These primers contained the *Nde*I and *Xho*I (underlined) restriction cleavage sites. The PCR reaction mixture contained the template DNA (∼0.1 μg), primers (4 μL of 25 μM), dNTPs (0.5 μL of 100 mM), $MgCl_2$ (10 μL of 25 mM), and *Pfu* DNA polymerase (1 μL of 2.5 units) in a total volume of 50 μL. The PCR reaction conditions were set as follows: 1 min at 95 °C for denaturation, 1 min at 55 °C for annealing, 2 min at 72 °C for extension, for a total number of 30 reaction cycles. The final products were allowed to extend for an additional 20 min. The PCR reaction product and the expression vector pET-20b (+) were digested with *Nde*I and *Xho*I and purified from an agarose gel using the Qiaquick gel extraction kit. The purified products were ligated by T4 DNA ligase and transformed into DH5α cells for plasmid propagation (*29*). The cloning of the coding regions of hCA I in the pET-20b(+) vector was confirmed by sequencing the plasmid at the University of Chicago Cancer Research Center. The plasmid vector containing the hCA I sequence has been named pET-hCA I.

Expression and Purification of Recombinant hCA I and Human Carbonic Anhydrase II (hCA II). The expression vector pMA-5−8 containing the hCA II gene (at the *Sma*I and *Bam*HI restriction cleavage sites) was obtained as a gift from Dr. Carol Fierke's laboratory. Both pET-hCA I and pMA-5−8 (hCA II) were transformed into *Escherichia coli* BL21 codon plus DE3(RIL) host cells by following the standard molecular biology protocol (*29*). The transformed cells were grown in LB medium, supplemented with 100 μg/mL of ampicillin, 5.0 μg/mL of chloramphenicol, and 60 μg/mL of $ZnSO_4$ at 37 °C until A_{600} was 0.6. The expression of hCA I and II was induced by addition of 400 μM IPTG and 400 μM $ZnSO_4$. The cells were incubated further at 25 °C overnight. The cells were centrifuged at 5000*g* for 15 min. The pellet was washed in 20 mM Tris-HCl at pH 8.7 and resuspended in the same buffer, containing 0.5 mM EDTA. A working concentration of 1 mM PMSF in 2-propanol was added prior to sonication. The cells were sonicated for a total time of 10 min in a Branson bath sonifier utilizing 40% duty cycle in an ice-cold bath. The sonicated extract was centrifuged at 15 000 rpm for 30 min, and the supernatant (crude extract) was collected for further purification. The recombinant forms of hCA I and II were purified from the crude extract as described by Banerjee et al. (*32*). During the course of purification, the protein concentration was determined by the Bradford method, utilizing BSA as the standard protein (*31*).

The concentrations of purified enzymes were determined spectrophotometrically using $\epsilon_{280} = 49$ and 54 mM^{-1} cm^{-1} based on MW = 30 000 for hCA I and II, respectively. The purified enzymes were judged to be homogeneous by the SDS−PAGE analysis.

The enzyme activity of the recombinant hCA I and II was measured in 25 mM HEPES buffer at pH 7.0 containing 10% acetonitrile (the standard buffer) at 25 °C, utilizing 0.4 mM *p*-nitrophenyl acetate as the substrate (*30*).

Spectrofluorometric Studies. All of the spectrofluorometric studies involving dansylamide were performed on a Perkin−Elmer lambda 50-B spectrofluorometer equipped with a

magnetic stirrer and thermostated water bath. To ensure the stability of dansylamide during the course of the titration as well as kinetic experiments, its stock solution (1 mM) was prepared in 10 mM HCl and it was diluted in the standard HEPES buffer containing 10% acetonitrile. The emission spectra of dansylamide in the absence and presence of hCA I and II were acquired by fixing the excitation wavelength at 330 nm, and both excitation and emission slits were maintained at 5 mm with a cutoff filter at 390 nm.

The dissociation constants of the hCA I−dansylamide and hCA II−dansylamide complexes were determined by titrating a fixed concentration of the enzyme (1 μM) with increasing concentrations of dansylamide in different pH buffers, containing 10% acetonitrile. The initial reaction volume was 2.0 mL. To maximize the signal-to-noise ratio as well as to minimize the fluorescence drift (contributed by the instability of dansylamide in our buffer system), we maintained the excitation and emission wavelengths to be 330 and 448 nm, respectively. The excitation and emission slits were 5 mm each. The dissociation constant of the enzyme−dansylamide complex was determined by analyzing the binding isotherm as described by Lesburg et al. (*33*).

The pK_a was determined by plotting different K_d values of the hCA I−dansylamide and hCA II−dansylamide complexes as a function of pH and analyzing according to the Henderson−Hasselbalch equation for a single proton equilibration process.

Transient Kinetic Experiments. To delineate the complete microscopic pathways for the binding of dansylamide to hCA I and II, we performed the stopped-flow transient kinetic studies. Transient kinetic experiments were performed on an Applied Photophysics SX-18 MV stopped-flow system, equipped with both absorption- and fluorescence-detecting photomultiplier tubes. The dead time of the stopped flow was 1.3 ms. For the fluorescence measurement, the light path was configured such that the fluorescence photomultiplier detected the emitting light through a 2 mm path length. The excitation wavelength was maintained at 330 nm, and a 395 nm cutoff filter was installed at the entrance of the photomultiplier tube. The stopped-flow traces were analyzed by the data analysis package provided by Applied photophysics.

pH Jump Relaxation Studies. These experiments were performed by mixing a solution of the enzyme−dansylamide complex, maintained at one pH, with a concentrated buffer at the other pH in the stopped-flow syringes, and recording the fluorescence change as described above. For a low to high pH jump, syringe A contained 2 μM hCA I/hCA II and 30 μM dansylamide in 5 mM MES buffer at pH 6.0 containing 10% acetonitrile and syringe B contained 150 mM Tris at pH 8.0 with 10% acetonitrile. Upon mixing, the pH of the solution changed to pH 7.9. For a high to low pH jump experiment, syringe A contained 2 μM hCA I/hCA II and 30 μM dansylamide in 5 mM Tris at pH 8.0 having 10% acetonitrile and syringe B contained 150 mM MES at pH 6.0 with 10% acetonitrile. Upon mixing, the pH of the mixture changed to 6.1.

Molecular-Modeling Studies. The molecular-modeling studies were performed on a Silicon Graphics-O2 molecular-modeling workstation with the aid of Accelrys software, InsightII(98). The coordinates for the X-ray crystallographic structures of bovine CA II complexed with dansylamide (1okl), hCA II complexed with 4-fluorobenzenesulfonamide (1IF4), and hCA I complexed with acetazolamide (1azm) were downloaded from Research Collaboratory for Structural Bioinformatics (RCSB) Protein Data Bank. The backbones of these proteins were superimposed, and the relative orientations of sulfonamide ligands were compared with the aid of InsightII software (Accelrys Inc.).

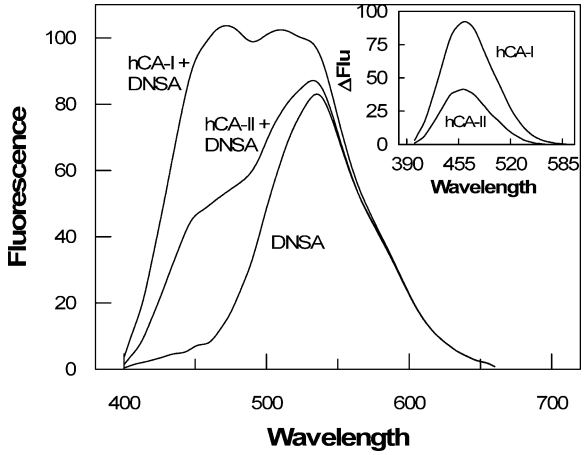

FIGURE 1: Fluorescence emission spectra of dansylamide. The emission spectra of dansylamide in the absence and presence of hCA I and II were taken in 25 mM HEPES buffer at pH 7.0 containing 10% acetonitrile. [Dansylamide] = 30 μM, [hCA I] = 1 μM, and [hCA II] = 1 μM. λ_{ex} = 330 nm, and cutoff filter = 390 nm. The inset shows the difference spectra, generated by subtracting the spectrum of free dansylamide from the spectra of the enzyme−dansylamide complexes.

RESULTS

Spectra and Binding Isotherms of the Enzyme−Dansylamide Complexes. Figure 1 shows comparative spectral features of dansylamide upon binding with hCA I and II. For the magnitude of the spectral changes to not be dominated by differential occupancy of the enzymes by the ligand, we used saturating concentrations of dansylamide in this experiment. As observed by others, the fluorescence emission spectrum of dansylamide (λ_{ex} = 330 nm and λ_{em} = 536 nm) is blue-shifted upon binding with both hCA I and II (*34*−*36*). Although the magnitude of the spectral shift remains more or less the same with both isozymes, the amplitude of the fluorescence emission is more pronounced in the case of hCA I as compared to hCA II. This is clearly noted in the difference spectra (the spectra of the enzyme−dansylamide complexes minus the individual species) shown in the inset of Figure 1. Because both hCA I and II were saturated by dansylamide, the origin of the above spectral difference must lie in the difference in microscopic environment of the active sites of the enzymes. The difference spectra of the hCA I−dansylamide and hCA II−dansylamide complexes exhibit the emission maxima at 458 and 455 nm, respectively. These values are somewhat lower than that reported by Chen and Kernohan (*34*), and the origin of such a difference may lie in the experimental conditions, instrumental setups, and the biological origin of the enzymes. However, because the fluorescence emission intensity of free dansylamide was minimal at 448 nm, we opted to use the latter emission wavelength for performing all of the titration and transient kinetic experiments, so that the signal-to-noise ratio is maximized and the fluorescence interference caused by the instability of dansylamide under our buffer solution is minimized (*11*).

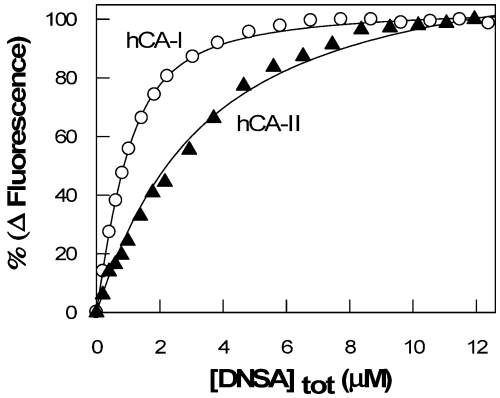

FIGURE 2: Binding isotherms for the interactions of dansylamide with hCA I and II. Other experimental conditions are the same as in Figure 1. The increase in the fluorescence emission intensity at 448 nm (λ_{ex} = 330 nm, and "cutoff" filter = 390 nm) for the titration of a fixed concentration of the individual enzyme (1 μM) as a function of the total concentration of dansylamide is shown. The solid smooth lines are the best fit of the data (*43*) for the K_d values of the hCA I−dansylamide and hCA II−dansylamide complexes as being equal to 0.46 ± 0.01 μM (○) and 2.74 ± 0.075 μM (▲), respectively.

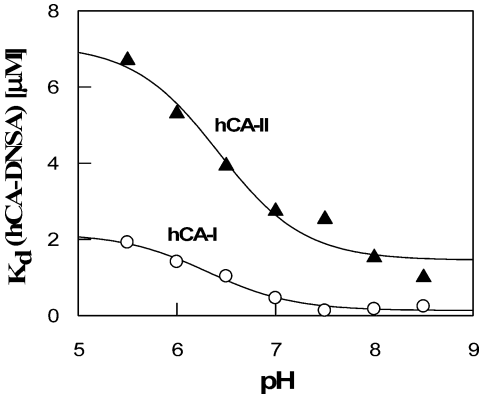

FIGURE 3: pH dependence of the dissociation constants (K_d) of the hCA−dansylamide complexes. The K_d values of the hCA−dansylamide complexes were determined as described in the caption of Figure 2. The solid smooth lines are the best fit of the experimental data according to the Henderson−Hasselbalch equation (for a single-proton equlibration process) with the pK_a values of 6.3 ± 0.13 and 6.4 ± 0.18 for hCA I−dansylamide and hCA II−dansylamide complexes, respectively.

Figure 2 shows the titration of fixed concentrations of hCA I and II by increasing concentrations of dansylamide, monitoring the increase in fluorescence emission at 448 nm (λ_{ex} = 330 nm). The solid smooth lines are the best fit of the experimental data for the dissociation constants of hCA I−dansylamide and hCA II−dansylamide complexes as being equal to 0.46 and 2.7 μM, respectively. Day et al. recently determined the K_d value of the bovine CA II−dansylamide complex by surface plasmon resonance, isothermal titration calorimetry, and stopped-flow kinetic methods, in PBS buffer at pH 7.4 and found its magnitude in the range between 0.34 and 0.42 μM (*36*). To ascertain whether the noted discrepancy between our data and those of Day et al. were due to the difference in the enzyme species (i.e., bovine versus human CA II) or the buffer type (i.e., PBS versus HEPES), we performed the binding studies of dansylamide with commercially available bovine CA II, exactly under our experimental condition. The K_d value of the bovine CA II−dansylamide complex, under our experimental condition, was found to be 0.84 μM. Clearly, the binding constant of the enzyme−dansylamide complex is dependent on both the enzyme type and the experimental conditions.

However, upon comparison of the K_d values of the hCA I−dansylamide and hCA II−dansylamide complexes under an identical experimental condition (Figure 2), it is obvious that, unlike other sulfonamide derivatives (*25*−*27*), dansylamide interacts about 6-fold more tightly with hCA I than with hCA II. This feature appears to be qualitatively similar to the higher amplitude of fluorescence changes upon binding of dansylamide with hCA I as compared to that with hCA II (see Figure 1). The question arose whether the origin of the corresponding spectral and binding profiles of hCA−dansylamide interactions was dictated by some common molecular mechanism.

Because the binding of dansylamide to hCAs was expected to be given, at least in part, by the protonation state of the ligand and/or the active-site groups of the enzyme, we determined the influence of pH on the K_d values of the hCA−dansylamide complexes (Figure 3). Note that as the pH increases, the K_d values of both the hCA I−dansylamide and hCA II−dansylamide complexes decrease. The solid smooth lines of Figure 3 are the best fit of the data according to the Handerson−Hasselbalch equation for the pK_a values of the hCA I−dansylamide and hCA II−dansylamide complexes as being equal to 6.3 and 6.4, respectively. Note a marked similarity in these pK_a values. Such a similarity attests to the fact that there is no energetic difference in protonation/deprotonation states of dansylamide and/or its interacting active-site residues of hCA I versus hCA II.

Transient Kinetics for the Enzyme−Dansylamide Interactions. To delineate the complete microscopic pathways for the binding of dansylamide to hCA I versus hCA II, we performed detailed stopped-flow transient kinetic experiments. During these measurements, the stopped-flow system was configured in the fluorescence detection mode, for the excitation via the 1 mm path length (λ_{ex} = 330 nm) and the emission via 2 mm path length (with a cutoff filter of 395 nm). Because the fluorescence changes upon binding of dansylamide to both hCA I and II were most pronounced at pH 8.0, we performed the initial transient kinetic experiments at this pH value. Figure 4 shows the time-dependent increase in the fluorescence signals upon mixing of hCA I and II with dansylamide (under a pseudo-first-order condition) via the stopped-flow syringes. The solid smooth lines are the best fit of the data according to the single-exponential rate equation for the relaxation rate constants ($1/\tau$) of 0.45 and 0.75 s^{-1} for the binding of dansylamide to hCA I and II, respectively.

To probe as to the extent of the observed florescence changes occurring during the dead time (1.3 ms) of our stopped flow, we performed a blank experiment. In this experiment, 10 μM dansylamide was mixed with the buffer while maintaining the photomultiplier voltage (726 V), identical to that utilized during the relaxation experiment for the binding of dansylamide to hCA I. The horizontal trace (control) of Figure 4 shows the time course of the fluorescence signal (which remains nearly constant as a function of time, 1.7 mV) under the above experimental condition. It should be noted that the latter value is similar to the

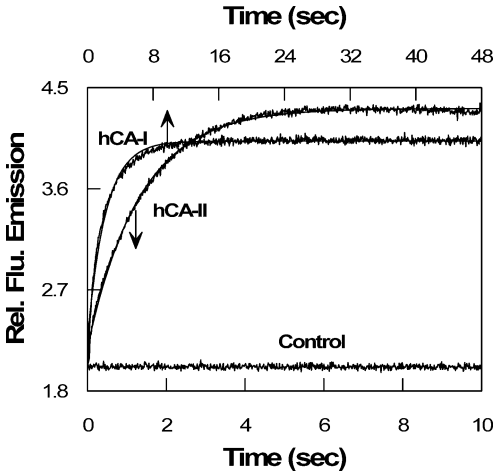

FIGURE 4: Representative stopped-flow traces for the interaction of dansylamide with hCAs. λ_{ex} = 330 nm, and "cutoff" filter = 395 nm. The after-mixing concentrations of hCA I, hCA II, and dansylamide were 0.5, 1, and 10 μM, respectively. The solid smooth lines are the best fit of the experimental data according to the single-exponential rate equation with rate constants of 0.45 ± 0.004 and 0.75 ± 0.0032 s^{-1} for hCA I and II, respectively. The control trace represents the sum of the fluorescence changes when dansylamide and hCA I are individually mixed against the buffer under the above experimental condition.

extrapolated single-exponential trace (for the interaction of dansylamide with hCA I) to the zero time (2.03 mV). This suggests that there is no fluorescence change upon binding of dansylamide to hCA I within 1.3 ms dead time of our stopped flow. In other words, all of the observed fluorescence changes occurred during the observed relaxation phase. As will be elaborated in the Discussion, this feature implies that the formation of the hCA I−dansylamide "encounter" complex does not accompany any change in the dansylamide fluorescence.

Dissociation "Off-Rates" of the Enzyme−Dansylamide Complexes. We performed the transient kinetic studies for the dissociation of dansylamide from the individual enzyme sites. In this experiment, a mixture of the enzyme−dansylamide complex was mixed with a high (and excessive) concentration of benzenesulfonamide via the stopped-flow syringes. Because benzenesulfonamide serves a competitive ligand of dansylamide, it displaces the latter from the enzyme site, leading to the diminution of the fluorescence signal of the enzyme-bound dansylamide (eq 1).

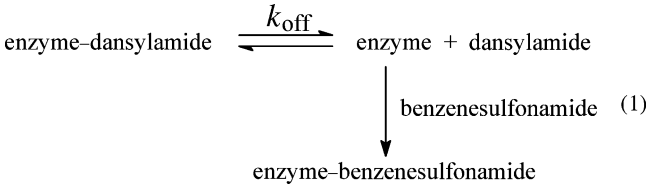

As per eq 1, the rate of formation of the enzyme−benzenesulfonamide complex would be limited by the rate of dissociation of dansylamide from its enzyme site, yielding the magnitude of the dissociation "off-rate" (k_{off}) of the enzyme−dansylamide complex. Figure 5 shows the stopped-flow traces for the dissociation of dansylamide from hCA I and II enzyme sites. The solid smooth lines are the best fit of the experimental data for the dissociation "off-rates" of dansylamide from hCA I and II sites as being equal to 0.025 and 0.17 s^{-1}, respectively. Note that unlike the association profiles (Figure 4), the dissociation "off-rate" of dansylamide from hCA I site is about 7-fold slower than that from the hCA II site. This difference is qualitatively similar to that obtained in the K_d values of the enzyme−ligand complexes (see Figure 2).

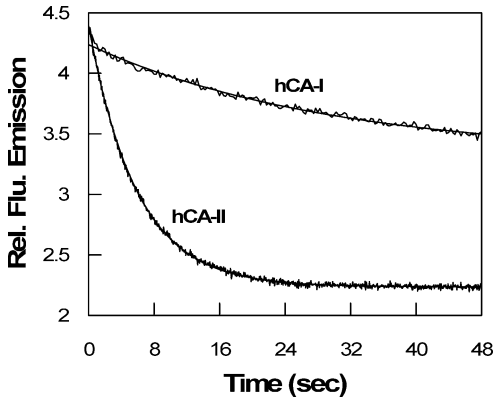

FIGURE 5: Representative stopped-flow traces for the dissociation of dansylamide from the hCA−dansylamide complexes. The dissociation of the enzyme-bound dansylamide was triggered upon mixing the hCA−dansylamide complexes with a high and excessive concentration of benzenesulfonamide at pH 8.0. The premixing concentrations of the individual species were as follows: [hCA I] = 0.5 μM + [dansylamide] = 10 μM versus [benzenesulfonamide] = 200 μM; [hCA II] = 4 μM + [dansylamide] = 40 μM versus [benzenesulfonamide] = 200 μM. The solid smooth lines are the best fit of the experimental data according to the single-exponential rate equation with the dissociation rate constant of 0.025 ± 0.0012 and 0.17 ± 0.0004 s^{-1} for hCA I and II, respectively.

Dansylamide Concentration Dependence of the Association Rate Constants of the Enzyme−Ligand Complexes. To delineate the microscopic pathways for the enzyme−dansylamide interaction, we performed the transient kinetics for the association of dansylamide with hCA I and II as a function of the ligand concentration. All of these experiments were performed under pseudo-first-order conditions ([hCA I/hCA II] ≪ [dansylamide]). Figure 6 shows the dansylamide concentration dependence of the observed relaxation rate constants ($1/\tau$). For both enzymes, as the concentration of dansylamide increases, the magnitude of $1/\tau$ increases. However, such an increase conforms to the hyperbolic dependence in the case of hCA I, but it conforms to the linear dependence in the case of hCA II. It should be pointed out that the observed linearity of the $1/\tau$ versus dansylamide plot in the case of hCA II was maintained up to a 80 μM concentration, and it was clearly distinct from the hyperbolic trend observed in the case of hCA I. The solid smooth lines are the best fits of the data for the hyperbolic dependence of $1/\tau$ on dansylamide (with offset) in the case of hCA I (Figure 6A) and linear dependence of $1/\tau$ on dansylamide in the case of hCA II (Figure 6B). The analysis of data of Figure 6A yielded the maximum ($1/\tau_{max}$) and minimum ($1/\tau_{min}$) relaxation rate constants and K_e values (the concentration of dansylamide required to achieve half of the maximum saturation of the enzyme) of 2.0 s^{-1}, 0.02 s^{-1}, and 43 μM, respectively. On the other hand, linear regression analysis of the data of Figure 6B yielded the slope and intercept values of 0.039 μM^{-1} s^{-1} and 0.37 s^{-1}, respectively.

We performed the above dansylamide concentration-dependent transient kinetic studies involving both enzymes at two additional pH values, viz., pH 6.0 and 7.0. Although

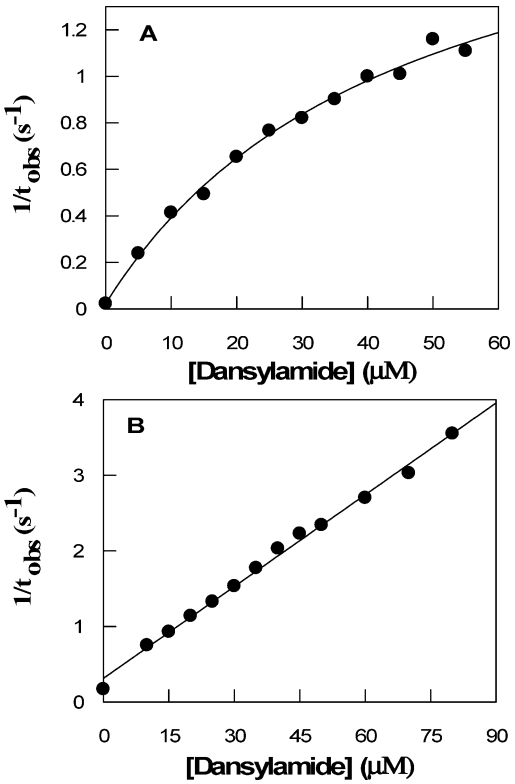

FIGURE 6: Dansylamide concentration dependence of the relaxation rate constants. The relaxation rate constants (determined under a pseudo-first-order condition) for the binding of dansylamide with hCA I and II were determined as a function of the ligand concentration. A and B represent the plots of $1/\tau_{obs}$ versus the dansylamide concentration involving hCA I and II, resepectively. Other conditions were same as in Figure 4. The after-mixing concentrations of hCA I (A) and hCA II (B) were 0.5 and 1 μM, respectively. The data at the zero concentration of dansylamide were taken from the dissociation off-rate measurements. The data of A have been analyzed for the hyperbolic dependence of the relaxation rate constant ($1/\tau_{obs}$) on the dansylamide concentration. The solid smooth line is the best fit of the data for the relaxation rate constants at the saturating concentration of dansylamide ($1/\tau_{max}$), the zero concentration of dansylamide ($1/\tau_{min} = k_{off}$), and the concentration of dansylamide required to achieve half of the maximal saturation (K_e) as being equal to 2.0 $\pm$ 0.23 s^{-1}, 0.02 $\pm$ 0.0002 s^{-1}, and 43 $\pm$ 9.6 μM, respectively. The solid line of B is the linear regression analysis of the data for the intercept and slope values of 0.37 $\pm$ 0.034 s^{-1} and 0.039 $\pm$ 0.0007 μM^{-1} s^{-1}, respectively.

Table 1: Summary of the pH-Dependent Macroscopic Parameters for the Binding of Dansylamide to hCA I

pH	$1/\tau_{max}$ (s^{-1})	$1/\tau_{min}$ (s^{-1})	K_e (μM)
6.0	3.4 $\pm$ 1.6	0.029 $\pm$ 0.000 16	177 $\pm$ 110
7.0	5.1 $\pm$ 1.2	0.023 $\pm$ 0.0002	163 $\pm$55
8.0	2.0 $\pm$ 0.23	0.02 $\pm$ 0.000 16	43 $\pm$ 9.6

the overall trend with the individual enzyme remained the same, the macroscopic parameters (particularly K_e value) for the enzyme−dansylamide interactions varied as a function of pH (Tables 1 and 2). As will be elaborated in the Discussion, the binding of dansylamide to both hCAs proceed via the two-step mechanism, of which the second step is differently (i.e., kinetically versus thermodynamically) controlled in the case of hCA I versus hCA II.

pH Jump Relaxation Studies. Given that the fluorescence emission intensity of the enzyme-bound dansylamide was more pronounced at pH 8.0 than at pH 6.0, a sudden change in pH between 8 and 6 was expected to alter the fluorescence

Table 2: Summary of the pH-Dependent Macroscopic Parameters for the Binding of Dansylamide to hCA II

pH	$1/\tau_{obs}$ (s^{-1}; intercept)	$1/\tau_{obs}$/[DNSA] (μM^{-1} s^{-1}; slope)
6.0	0.33 $\pm$ 0.016	0.013 $\pm$ 0.0003
7.0	0.25 $\pm$ 0.13	0.049 $\pm$ 0.0023
8.0	0.37 $\pm$ 0.034	0.039 $\pm$ 0.0007

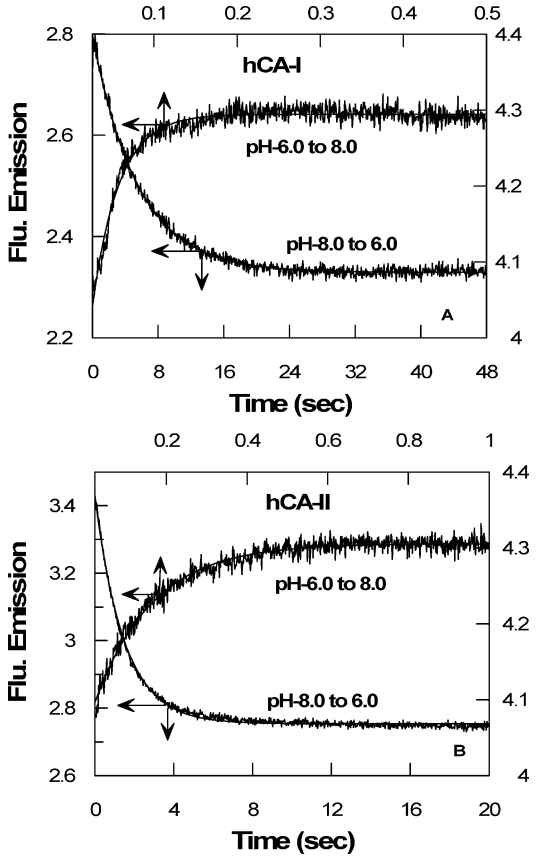

FIGURE 7: pH jump experiments of the hCA−dansylamide complexes. The stopped-flow traces of the hCA−dansylamide complexes upon mixing with buffers of selected pH values are shown. The pH jump from 8 to 6 was accomplished by mixing the hCA−dansylamide complex in 5 mM Tris buffer at pH 8.0 with 150 mM MES buffer at pH 6.0. The pH of the mixture was determined to be 6.1. For the pH jump from 6 to 8, the hCA−dansylamide complex in 5 mM MES buffer at pH 6.0 was mixed with 150 mM Tris buffer at pH 8.0. The pH of the mixture was found to be 7.9. A and B show the pH jump experiments involving hCA I and II, respectively. The solid smooth lines are the best fit of the data according to the single-exponential rate equation with the rate constants of 31.5 $\pm$ 0.5 s^{-1} (pH 6.0−8.0) and 0.18 $\pm$ 0.001 s^{-1} (pH 8.0−6.0) for hCA I (A), and 6.96 $\pm$ 0.096 s^{-1} (pH 6.0−8.0) and 0.67 $\pm$ 0.0034 s^{-1} (pH 8.0−6.0) for hCA II (B), respectively.

signals as a function of time. To determine the kinetics of the "pH jump" experiment, we mixed the hCA I−dansylamide complex in 5 mM Tris buffer at pH 8.0 with 150 mM MES buffer at pH 6.0 (the pH of the mixture emerged to be 6.1) via the stopped-flow syringes and monitored the time course of the fluorescence changes. Figure 7A shows the time-dependent decrease in fluorescence of the hCA I−dansylamide complex upon the pH jump from 8 to 6. An essentially identical experiment was performed for the mixing of the hCA I−dansylamide complex maintained at pH 6.0 with 150 mM Tris buffer at pH 8.0 (the pH of the mixture was 7.9). Note that the opposite pH jump (i.e., from 6.0 to

8.0) resulted in the time-dependent increase (Figure 7A) in the enzyme−dansylamide fluorescence. Both of the traces of Figure 7A conformed to the single-exponential rate equations, with the rate constants of 31.5 and 0.18 s^{-1}, respectively. We performed the similar experiment with the hCA II−dansylamide complex (Figure 7B), and the corresponding single-exponential rate constants were found to be 6.96 and 0.67 s^{-1}, respectively. Note that whereas the pH jump from 6 to 8 is kinetically more favorable in the case of hCA I than hCA II, the pH jump from 8 to 6 is more favorable in the case of hCA II than hCA I. We believe that the origin of the above differences lies in the energetics of the alternative pathways involved in the pH-dependent changes of the enzyme−dansylamide fluorescence.

DISCUSSION

The experimental data presented herein provide for the first time (to the best of our knowledge) a detailed account of the microscopic pathways for the binding of dansylamide to the active sites of hCA I and II. All arylsulfonamide derivatives (containing free amide nitrogen) are known to inhibit the CA-catalyzed reactions because of the binding at the active sites of the enzyme. Supuran and his collaborators compiled a list of more than 200 sulfonamide derivatives as CA inhibitors, of which most of them interact more tightly with hCA II than with hCA I, and only a few of them exhibit comparable binding affinity with both of these isozymes (*13*, *25*−*27*). Contrary to the above generality, dansylamide falls in the category of an unusual sulfonamide derivative, which interacts more tightly with hCA I than with hCA II. Clearly, the above difference must be encoded either in the structural feature of the enzyme, the active-site environment of the enzymes, or a combination of both of these features. Hence, understanding the molecular aspect of the enzyme−ligand interaction, particularly from the point of view of isozyme selectivity, is expected to provide insights into designing new class of CAs as potential drugs.

The experimental data presented in the previous section on the kinetic and thermodynamic disparities for the binding of dansylamide to hCA I versus hCA II lead to the following conclusions: (i) Although the binding of dansylamide to both hCA I and II results in an identical blue shift in its fluorescence emission spectrum, the amplitude of the fluorescence intensity is more pronounced in the case of hCA I than with hCA II (Figure 1). (ii) Unlike other sulfonamide derivatives (*25*−*27*), the binding affinity of dansylamide for hCA I is about 6-fold higher than that for hCA II (Figure 2). (iii) The dissociation "off-rate" of dansylamide from the hCA I site is about 7-fold slower than that from hCA II (Figure 5). (iv) Despite the above differences, the pK_a values of the enzyme−dansylamide complexes are nearly identical (Figure 3). (v) Whereas the relaxation rate constant ($1/\tau$) for the association of dansylamide to hCA I exhibits a hyperbolic dependence, the relaxation rate constant ($1/\tau$) for the association of dansylamide to hCA II exhibits a linear dependence (Figure 6). (vi) Whereas the pH jump from 6 to 8 is kinetically more favorable in the case of hCA I as compared to hCA II, the above process in the opposite direction (i.e., the pH jump from 8 to 6) is kinetically more favorable in the case of hCA II as compared to hCA I. These differences are explainable in light of the difference in the microscopic pathways for the binding of dansylamide with hCA I versus hCA II sites. As elaborated below, the initial binding of dansylamide to hCA I versus hCA II site (within the "encounter" complex) dictates the kinetic as well as thermodynamic feasibility of the enzyme−ligand isomerization step, with concomitant changes in the fluorescence of the enzyme-bound dansylamide.

Fluorescence Spectra and Binding Profiles of Dansylamide. The binding of dansylamide to CAs results in the blue shift in both absorption and fluorescence spectra, and such electronic spectral changes have been attributed to the nonpolar active-site environment of the enzymes (*34*). Because the binding of sulfonamide derivatives to the active-site Zn^{2+} of the enzyme results in the deprotonation of the NH_2 group, it is believed that the latter process, at least in part, contributes to the overall fluorescence spectral changes of the enzyme-bound dansylamide. Given these, it would intuitively appear that the marked disparity in the intensity of fluorescence emission of dansylamide upon binding to hCA I versus hCA II site is due to the difference in the pK_a value of the NH_2 group of dansylamide at these enzyme sites. However, this does not appear to be the case (see Figure 3).

The pK_a value of the amide group of free dansylamide has been determined to be 9.8 (*34*). Given that the active-site Zn^{2+} of CAs acts as Lewis acid and interacts fairly tightly with sulfonamide nitrogen (*37*), the pK_a value of the enzyme-bound dansylamide must be lower than that of free dansylamide. It is unclear as to the extent that the above interaction contributes to the overall binding affinity of sulfonamide derivatives for their cognate enzyme sites. The inhibition data of different sulfonamide derivatives versus their pK_a values provide no clue as to the contribution of the latter parameter in stabilization of the enzyme−ligand complexes (*37*). Hence, it appears likely that, aside from the energetic contributions of the Lewis acid−base pair between the active-site Zn^{2+} and deprotonated sulfonamide moiety of dansylamide, other noncovalent interactions (including hydrophobic forces) are involved in stabilizing the hCA I/hCA II−dansylamide complexes. At this point, we propose that the pK_a values of 6.3−6.4 derived from the K_d (hCA−dansylamide) versus pH plots (Figure 3) are contributed by the Zn^{2+}-bound dansylamide, although we cannot rule out the contribution of Zn^{2+}-bound water in the above parameter (*38*). Irrespectively, the observed difference in the spectral and binding profiles of the enzyme−dansylamide complexes are modulated by the microscopic environments of CA isozymes.

Microscopic Pathways for the Binding of Dansylamide. The fact that the relaxation rate constant for the binding of dansylamide to hCA I exhibits a hyperbolic dependence (Figure 6A) suggests that the overall binding mechanism proceeds via two steps (eq 2).

$$\overbrace{\text{hCA-I} + \text{DNSA} \underset{k_{-1}}{\overset{k_1}{\rightleftharpoons}} \text{hCA-I--DNSA}}^{\text{fast}} \overbrace{\underset{k_{-2}}{\overset{k_2}{\rightleftharpoons}} (\text{hCA-I -- DNSA})^*}^{\text{slow}} \quad (2)$$

encounter complex isomerized complex

Assuming that the enzyme−ligand interaction satisfies the rapid equilibrium condition (*39*), the observed relaxation phase is expected to be given by the second (slow) step. Of these two-step binding mechanisms, the first step involves the formation of the hCA I−dansylamide encounter complex ($K_e = k_{-1}/k_1$), which undergoes the slow relaxation process

to form the (hCA I−dansylamide)* isomerization complex. Because the extrapolated single-exponential phase to zero time coincides with the fluorescence emission intensity of the mixture of the enzyme and dansylamide (without direct interaction; the control horizontal trace of Figure 4), it is obvious that no fluorescence changes occur during the formation of the "encounter" complex. All of the fluorescence changes of dansylamide occur upon binding with hCA I during the second isomerization step of eq 2. We propose that the deprotonation of the amide nitrogen of dansylamide occurs during the above isomerization step. Although from the mechanistic point of view, the enzyme−ligand isomerization process is attributed to proceed in concomitance with the changes in the protein conformation (*40*), the latter does not need to be highly pronounced to produce the above effect. Even small adjustments in the side chains of the active-site resident amino acid residues or adjustments (e.g., protonation/deprotonation) in the ligand structures can provide evidence of the isomerization step during the course of enzyme−ligand interactions (*41*−*43*).

For the model of eq 2, the observed relaxation rate constant ($1/\tau_{obs}$) can be shown to be related to the microscopic parameters of the two-step binding process (eq 3). Of

$$1/\tau_{obs} = \frac{k_2[\text{DNSA}]}{K_e + [\text{DNSA}]} + k_{-2} \qquad (3)$$

different parameters of eq 3, k_{-2} serves as a measure of the dissociation "off-rate" (k_{off}) of dansylamide from hCA I, which has been independently determined by the benzenesulfonamide displacement method (Figure 5). When the dansylamide concentration-dependent $1/\tau_{obs}$ is analyzed by eq 3, we obtain the magnitudes of K_e (k_{-1}/k_1), k_2, and k_{-2}, which allow the prediction of the overall dissociation constant of the hCA I−dansylamide complex ($K_d = K_e k_{-2}/k_2$). The predicted K_d values from the relaxation kinetic data at pH 6, 7, and 8 were 1.6, 0.7, and 0.42 μM, respectively. These values are similar to the experimentally observed K_d values of 1.4, 0.5, and 0.17 μM at pH 6, 7, and 8, respectively. The above correspondence attests to the internal consistency of our two-step binding model.

In contrast to the hyperbolic dependence of $1/\tau_{obs}$ on dansylamide in the case of hCA I, the above parameter shows a linear dependence in the case of hCA II. Such a profile was surprising because the binding of benzenesulfonamide to the Co^{2+}-substituted enzyme shows a hyperbolic dependence on the ligand concentration (our unpublished results). Obviously, dansylamide exhibits a somewhat different behavior in regards to its binding with hCA II versus hCA I.

Although the linear dependence of $1/\tau_{obs}$ on the dansylamide concentration in the case of hCA II (Figure 6B) may imply a single-step binding process (*40*), it can be alternatively explained by the two-step mechanism, as proposed with hCA I (eq 2). However, to simplify the kinetic complexity, we assume that, of the two-step hCA II−dansylamide binding process, the second step is faster than the first step (k_1 and $k_{-1} < k_2$ and k_{-2}) as depicted by eq 4.

$$\overbrace{\text{hCA-II} + \text{DNSA} \underset{k_{-1}}{\overset{k_1}{\rightleftharpoons}} \text{hCA-II--DNSA}}^{\text{slow}} \overbrace{\underset{k_{-2}}{\overset{k_2}{\rightleftharpoons}} (\text{hCA-II -- DNSA})^*}^{\text{fast}} \qquad (4)$$

encounter complex isomerized complex

From the model of eq 4, the relationship between $1/\tau_{obs}$ and the dansylamide concentration can be given by eq 5.

$$1/\tau_{obs} = k_1[\text{DNSA}] + \frac{k_{-1}k_{-2}}{k_2 + k_{-2}} \qquad (5)$$

Although eq 5 predicts a linear dependence of $1/\tau_{obs}$ as a function of the dansylamide concentration (Figure 6B), because of uncertainty in the magnitudes of k_2 and k_{-2}, we could not reliably predict the overall dissociation constant of the hCA II−dansylamide complexes at different pH values. It should be pointed out that, if $k_{-2} \gg k_2$, the isomerized complex would be insignificant and the overall binding mechanism would be reduced to the one-step process. On the other hand, if is k_2 is comparable to or slightly higher than k_{-2}, only a small fraction of the enzyme−ligand encounter complex is expected to be isomerized and most of the enzyme would predominate as the enzyme−ligand encounter complex. Because in the case of dansylamide, only the enzyme−ligand isomerized complex yields the characteristics fluorescence signal and its amplitude is smaller with hCA II than with hCA I, it appears evident that k_2/k_{-2} is less favorable in the case of hCA II than with hCA I. Hence, whereas the isomerization equilibrium of the enzyme−dansylamide complex is kinetically favorable and thermodynamically opposed in the case of hCA II, it is thermodynamically favorable but kinetically opposed in the case of hCA I. Given this scenario, dansylamide is expected to predominate more in the form of the enzyme−ligand isomerized complex in the case of hCA I than in the form of the enzyme−ligand "encounter" complex in the case of hCA II. This is presumably why the fluorescence spectral changes of the hCA I−dansylamide complex are more pronounced than those of the hCA II−dansylamide complex. This feature appears to be unique with dansylamide and not with benzenesulfonamide, because our transient kinetic data suggest that the latter compound is stabilized in the isomerized conformational state of hCA II.

Structural Basis of Enzyme−Ligand Interactions. Examination of the X-ray crystallographic structures of hCA I and II in the absence and presence of bound ligands reveals that the active-site pockets of these enzymes are predominantly hydrophobic and the ligand binding does not involve major changes in the protein conformation (*44*). However, some local changes in various side-chain amino acids within the active-site pockets of these enzymes are noteworthy, and such changes have been ascribed to help in accommodating structurally different types of ligands at the active sites of these isozymes (*44*). The fact that bovine CA II-bound dansylamide is differently oriented (versus other arylsulfonamide derivatives) within the active site of the enzyme (*28*) is evident from the comparative structural data of Figure 8. Instead of a normal mode of interaction with other sulfonamide derivatives, dansylamide preferentially binds more toward the hydrophobic region of the active site of the enzyme, and its naphthalene ring is twisted around 54° from the aromatic ring of other derivatives (*28*). We attribute that the unique binding mode of dansylamide at the active site of CA II is due to the predominance of the enzyme-bound dansylamide in the conformational state of the "encounter" complex (eq 4). We surmise that, because other arylsulfonamides (bound to hCA II) are favorably transi-

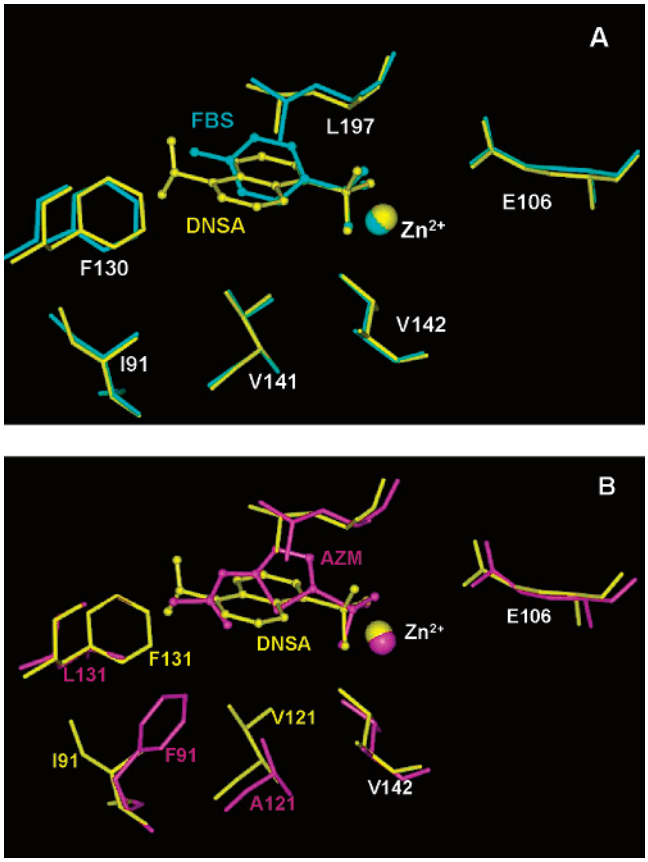

FIGURE 8: Orientation of dansylamide within the active site of bovine CA II. The spatial relationship of dansylamide bound to bovine CA II is compared with that of 4-fluorobenzenesulfonamide bound to hCA II (A) as well as with acetazolamide bound to hCA I (B). The selected amino acid residues in 5 Å vicinity of the sulfonamide derivatives of both enzyme structures are shown.

tioned from the "encounter complex" to the "isomerized complex" conformational states, they are differently orientated in the crystallographic structures (*44*). As per our mechanistic model, we predict that the crystal structure of the hCA I−dansylamide complex would show the normal mode of binding of dansylamide at the active site of the enzyme.

The binding of a ligand to its cognate enzyme site can be envisaged to proceed in three steps, namely, desolvation, immobilization, and packing (*46*). On kinetic grounds, the first two processes are expected to proceed concomitantly. On the basis of the enzyme and/or the ligand type, any of the above steps can be faster. Usually "packing" is expected to occur on a longer time scale particularly because it involves sampling of alternative conformational states of both protein and ligand molecules. In the case of hCA I and dansylamide (and possibly other sulfonamide derivatives), the slower isomerization step is likely to be a consequence of packing of the individual atoms of the enzyme and ligands to yield optimally bonded and maximally stable structures of the enzyme−ligand complexes. If an enzyme can accommodate structurally different ligands, the extent of packing would be expected to be different with different ligands. Likewise, if a mutation creates a "void" at or near the active site of an enzyme and such a void is not filled by a water molecule, the magnitude of packing of the individual enzyme−ligand complexes would be different with wild type versus the mutant enzyme. In the case of hCA II, dansylamide appears to be stabilized within the "immobilized" state (similar to the kinetically derived "encounter" complex), and thus, the subsequent "packing" (similar to the kinetically derived "isomerization") step is obviated. In this regard, it appears evident that the enzyme conformational and ligand structural states are intimately coupled.

In attempting to rationalize the structural−functional aspects of enzyme−dansylamide interactions, we note that, unlike most of the sulfonamide derivatives (which contain single five- or six-membered aromatic rings), dansylamide contains two fused six-membered aromatic rings. In addition, there is an electron-donating dimethylamino group that can acquire partially positive charge because of delocalization of electrons under the influence of electrophillic Zn^{2+} (interacting with the sulfonamide nitrogen). Hence, the overall stability as well as orientation of dansylamide (versus other sulfonamide derivatives) within the active-site pockets of CAs would be a consequence of several opposing/synergistic forces. It has been observed that several site-specific mutations (e.g., Leu-198 → Ala) that create a "void" within the active-site pocket of the enzyme facilitate the interaction of dansylamide (*35*). In this regard, it is noteworthy that the active-site pocket of hCA I contains a few shorter side-chain-containing amino acids than those found in the case of hCA II (*45*). For example, the active-site residues Val-121, Phe-131, and Val-135 of hCA II are substituted by Ala-121, Leu-131, and Ala-135, respectively, in the case of hCA I. These less bulky residues at the active-site pocket of hCA I may facilitate accommodation of the bulky aromatic ring of dansylamide within the enzyme−ligand encounter complex. However, because of technical reasons, we could not test this hypothesis by performing the energy minimization of the hCA I−dansylamide complex. We conjecture that the isomerization of the encounter complex would involve a change in the protein conformation, leading to narrowing of the active-site pocket and stabilizing the ultimate hCA I−dansylamide complex. Because we could not detect any change in the secondary structural elements of the enzymes upon binding with dansylamide via CD spectroscopy (our unpublished results), we believe our kinetically derived protein conformational changes must be subtle and restricted at the tertiary structural level. However, at this time, we cannot rule out the possibility of other long-range interactions that remain elusive in the X-ray crystallographic structures of the enzyme−ligand complexes. Given these, it is conceivable that a combination of the structural and mechanistic features of the enzyme−ligand interactions is required to understand the molecular basis of enzyme specificity. These are particularly important from the point of view of rationally designing the isozyme-specific inhibitors as potential drugs against CAs, as well as other pathogenic enzymes.

REFERENCES

1. Palmer, R. A., and Niwa, H. (2003) X-ray crystallographic studies of protein−ligand interactions, *Biochem. Soc. Trans. 31*, 973−979.
2. Miao, J., Chapman, H. N., Kirz, J., Sayre, D., and Hodgson, K. O. (2004) Taking X-ray diffraction to the limit: Macromolecular structures from femtosecond X-ray pulses and diffraction microscopy of cells with synchrotron radiation, *Annu. Rev. Biophys. Biomol. Struct. 33*, 157−176.
3. Pickford, A. R., and Campbell, I. D. (2004) NMR studies of modular protein structures and their interactions, *Chem. Rev. 104*, 3557−3566.

4. Buchanan, S. G. (2002) Structural genomics: Bridging functional genomics and structure-based drug design, *Curr. Opin. Drug Discovery Dev. 5*, 367−381.
5. Davis, A. M., Teague, S. J., and Kleywegt, G. J. (2003) Application and limitations of X-ray crystallographic data in structure-based ligand and drug design, *Angew Chem., Int. Ed. 42*, 2718−2736.
6. Berman, H. M., Westbrook, J., Feng, Z., Gilliland, G., Bhat, T. N., Weissig, H., Shindyalov, I. N., and Bourne, P. E. (2000) The Protein Data Bank, *Nucleic Acids Res. 28*, 235−242.
7. Lolis, E., and Petsko, G. A. (1990) Transition-state analogues in protein crystallography: Probes of the structural source of enzyme catalysis, *Annu. Rev. Biochem. 59*, 597−630.
8. Benkovic, S. J., and Somorjai, G. A. (2001) Future directions of catalysis science workshop, *Catal. Lett. 76*, 111−124.
9. Sawaya, M. R., and Kraut, J. (1997) Loop and subdomain movements in the mechanism of *Escherichia coli* dihydrofolate reductase: Crystallographic evidence, *Biochemistry 36*, 586−603.
10. Roy, B. C., Hegge, R., Rosendahl, T., Jia, X., Lareau, R., Mallik, S. and Srivastava, D. K. (2003) Conjugation of poor inhibitors with surface binding groups: A strategy to improve inhibition, *J. Chem. Soc., Chem. Commun. 18*, 2328−2329.
11. Banerjee, A. L., Swanson, M., Roy, B. C., Jia, X., Haldar, M., Mallik, S., and Srivastava, D. K. (2004) Protein surface-assisted enhancement in the binding affinity of an inhibitor for recombinant human carbonic anhydrase II, *J. Am. Chem. Soc. 126*, 10875−10883.
12. Roy, B. C., Banerjee, A. L., Swanson, M., Jia, X. G., Haldar, M. K., Mallik, S., Srivastava, D. K. (2004) Two-prong inhibitors for human carbonic anhydrase, *J Am. Chem. Soc. 126*, 13206−13207.
13. Supuran, C. T., Scozzafava, A., and Conway, J. (2004) Carbonic anhydrase: Its inhibitors and activators, CRC Press, Boca Raton, FL.
14. Supuran, C. T., Scozzafava, A., and Casini, A. (2003) Carbonic anhydrase inhibitors, *Med. Res. Rev. 23*, 146−189.
15. Nishimoiri, I. (2004) Acatalytic CAs: Carbonic anhydrase related proteins, in *Carbonic Anhydrase: Its Inhibitors and Activators* (Supuran, C. T., Scozzafava, A., and Conway, J., Eds.) pp 24−43, CRC Press, Boca Raton, FL.
16. Chegwidden, W. R., and Carter, N. D. (2000) *The Carbonic Anhydrases: New Horizons*, Birkhauser Verlag, Basel, Switzerland.
17. Scozzafava, A., Mastrolorenzo, A., and Supuran, C. T. (2004) Modulation of carbonic anhydrase activity and its applications in therapy, *Expert Opin. Ther. Pat. 14*, 667−702.
18. Schuman, J. (2002) Short- and long-term safety of glaucoma drugs, *Expert Opin. Drug Saf. 1*, 181−194.
19. Gray, W. D. and Rauh, C. E. (1967) The anticonvulsant action of inhibitors of carbonic anhydrase: Site and mode of action in rats and mice, *J. Pharmacol. Exp. Ther. 156*, 383−396.
20. Scozzafava, A., Mastrolorenzo, A., and Supuran, C. T. (2004) Modulation of carbonic anhydrase activity and its applications in therapy, *Expert Opin. Ther. Pat., 14*, 667−702.
21. Barnish, I. T., Cross, P. E., Dickinson, R. P., Gadsby, B., Parry, M. J., Randall, M. J., and Sinclair, I. W. (1980) Cerebrovasodilatation through selective inhibition of the enzyme carbonic anhydrase.2.imidazo[2,1-β]thiadiazole and imidazo[2,1-β]thiazole-sulfonamides, *J. Med. Chem.* 23, 117−121.
22. Peters, G., and Roch-Ramel, F. (1969) Thaiziide diuretics and related drugs, in *Handbook of Experimental Pharmacology*, Vol. 24, pp 257−385.
23. Pastorekova, S., Parkkila, S., Pastorek, J., and Supuran, C. T. (2004) Carbonic anhydrases: Current state of the art, therapeutic applications, and future prospects, *J. Enzyme Inhib. Med. Chem. 19*, 199−229.
24. Herklel, U., and Pfeiffer, N. (2001) Update on topical carbonic anhydrase inhibitors, *Curr. Opin. Ophthalmol. 12*, 88−93.
25. Supuran, C. T., and Scozzafava, A. (2002) Applications of carbonic anhydrase inhibitors and activators in therapy, *Expert Opin. Ther. Pat. 12*, 217−242.
26. Scozzafava, A., Menabuoni, L., Mincione, F., and Supuran, C. T. (2002) Carbonic anhydrase inhibitors. A general approach for the preparation of water-soluble sulfonamides incorporating polyamino-polycarboxylate tails and of their metal complexes possessing long-lasting, topical intraocular pressure-lowering properties, *J. Med. Chem. 45*, 1466−1476.
27. Vullo, D., Franchi, M., Gallori, E., Antel, J., Scozzafava, A., and Supuran, C. T. (2004) Carbonic anhydrase inhibitors. Inhibition of mitochondrial isozyme V with aromatic and heterocyclic sulfonamides, *J. Med. Chem. 47*, 1272−1279.
28. Nair, S. K., Elbaum, D., and Christianson, D. W. (1996) Unexpected binding mode of the sulfonamide fluorophore 5-(dimethylamino)-1-naphthalene sulfonamide to human carbonic anhydrase II. Implications for the development of a zinc biosensor, *J. Biol. Chem. 271*, 1003−1007.
29. Sambrook, J., Fritsch, E. F., and Maniatis, T. (2000) *Molecular Cloning: A Laboratory Manual*, Cold Spring Harbor Press, Cold Spring Harbor, New York.
30. Pocker, Y., and Stone, J. T. (1967) Catalytic versatility of erythrocyte carbonic anhydrase III. Kinetic studies of the enzyme-catalyzed hydrolysis of *p*-nitrophenyl acetate, *Biochemistry 6*, 668−678.
31. Bradford, M. M. (1976) A rapid and sensitive method for the quantitation of microgram quantities of protein utilizing the principle of protein-dye binding, *Anal. Biochem. 72*, 248−254.
32. Banerjee, A. L., Swanson, M., Mallik, S., and Srivastava, D. K. (2004) Purification of recombinant human carbonic anhydrase II by metal affinity chromatography without incorporating Histidine tags, *Protein Expression Purif. 37*, 450−454.
33. Lesburg, C. A., Huang, C.-C., Christianson, D. W., and Fierke, C. A. (1997) Histidine → carboxamide ligand substitution in the zinc binding site of carbonic anhydrase II after metal coordination geometry but retain catalytic activity, *Biochemistry 36*, 15780−15791.
34. Chen, R. F., and Kernohan, J. C. (1967) Combination of bovine carbonic anhydrase with a fluorescent sulfonamide, *J. Biol. Chem.* 242, 5813−5823.
35. Nair, S. K., Krebs, J. F., Christianson, D. W., and Fierke, C. A. (1995) Structural basis of inhibitor affinity to variants of human carbonic anhydrase II, *Biochemistry 34*, 3981−3989.
36. Day, Y. S. N., Baird, C. L., Rich, R. L., and Myszka, D. G. (2002) Direct comparison of binding equilibrium, thermodynamic, and rate constants determined by surface- and solution-based biophysical methods, *Protein Sci. 11*, 1017−1025.
37. Supuran, C. T., Casini, A., and Scozzafava, A. (2004) Development of sulfonamide carbonic anhydrase inhibitors, in *Carbonic Anhydrase: Its Inhibitors and Activators* (Supuran, C. T., Scozzafava, A., and Conway, J., Eds.) pp 67−147, CRC Press, Boca Raton, FL.
38. Earnhardt, J. N., Qian, M., Tu, C., Lakkis, M. M., Bergenhem, N. C., Laipis, P. J., Tashian, R. E., and Silverman, D. N. (1998) The catalytic properties of murine carbonic anhydrase VII, *Biochemistry 37*, 10837−10845.
39. Hammes, G. G. (1982) *Enzyme Catalysis and Regulation*, Academic Press, New York.
40. Bernasconi, C. F. (1976) *Relaxation Kinetics*, Academic Press, New York.
41. Johnson, J. K., and Srivastava, D. K. (1993) Detection and identification of a chromophoric intermediate during medium chain fatty acyl CoA dehydrogenase catalyzed reaction via rapid-scanning UV/visible spectroscopy, *Biochemistry, 32*, 8004−8013.
42. Kumar, N. R., and Srivastava, D. K. (1994) Reductive half-reaction of medium-chain fatty acyl-CoA dehydrogenase utilizing octanoyl-CoA/octenoyl-CoA as a physiological substrate/product pair: Similarity in the microscopic pathways of octanoyl-CoA oxidation and octenoyl-CoA binding, *Biochemistry 33*, 8833−8841.
43. Qin, L., and Srivastava, D. K. (1998) Energetics of two-step binding of a chromophoric reaction product, *trans*-3-indoleacryl-oyl-CoA, to medium chain acyl-CoA dehydrogenase, *Biochemistry 37*, 3499−3508.
44. Stams, T., and Christianson, D. W. (2000) X-ray crystallographic studies mammalian carbonic anhydrase isozymes, in *The Carbonic Anhydrases: New Horizons* (Chegwidden, W. R., Carter, N. D., and Edwards, Y., Eds.) Vol. 90, pp 159−174, Springer-Verlag, New York.
45. Chakravarty, S., and Kannan, K. K. (1994) Drug−protein interactions. Refined structures of three sulfonamide drug complexes of human carbonic anhydrase I enzyme, *J. Mol. Biol. 243*, 298−309.
46. Morton, A., Baase, W. A., and Matthews, B. W. (1995) Energetic origins of specificity of ligand binding in an interior nonpolar cavity of T4 lysozyme, *Biochemistry 34*, 8564−8575.

BI0475018